Journal of the mechanical behavior of biomedical materials 66 (2017) 181–186

Contents lists available at ScienceDirect

Journal of the Mechanical Behavior of Biomedical Materials

journal homepage: www.elsevier.com/locate/jmbbm

Strain shielding in trabecular bone at the tibial cement-bone interface

Priyanka Srinivasan[a,*], Mark A. Miller[b], Nico Verdonschot[a,c], Kenneth A. Mann[b], Dennis Janssen[a]

[a] Orthopaedic Research Laboratory, Radboud Institute for Health Sciences, Radboud university medical center, Nijmegen, The Netherlands
[b] Department of Orthopedic Surgery, SUNY Upstate Medical University, Upstate Medical University, 3216 IHP, 750 East Adams Street, Syracuse, NY 13210, USA
[c] University of Twente, Laboratory for Biomechanical Engineering, Faculty of Engineering Technology, Enschede, The Netherlands

ARTICLE INFO

Keywords:
Bone-cement interface
Strain shielding
Micromotion
Aseptic loosening
Finite element analysis

ABSTRACT

Aseptic loosening of the tibial component remains the leading cause for revision surgery in total knee arthroplasty (TKA). Understanding the mechanisms leading to loss of fixation can offer insight into preventative measures to ensure a longer survival rate. In cemented TKA, loosening occurs at the cement-trabecular interface probably due to a stress-shielding effect of the stiffer implant material in comparison with bone. Using finite element models of lab-prepared tibial cement-trabeculae interface specimens (n=4) based on micro-CT images, this study aims to investigate the micromechanics of the interlock between cement and trabecular bone. Finite element micromotion between cement and trabeculae and bone strain were compared in the interdigitated trabeculae as well as strain in the bone distal to the interface. Lab-prepared specimens and their FE models were assumed to represent the immediate post-operative situation. The cement layer was removed in the FE models while retaining the loading conditions, which resulted in FE models that represented the pre-operative situation. Results showed that micromotion and bone strain decrease when interdigitation depth increases. Bone-cement micromotion and bone strain at the distal interdigitated region showed a dependence on bone volume fraction. Comparing the immediate post-operative and pre-operative situations, trabeculae embedded deep within the cement generally showed the highest level of strain-shielding. Strain shielding of interdigitated bone, in terms of reduction in compressive strains, was found to be between 35 and 61 % for the four specimens. Strain adaptive remodeling could thus be a plausible mechanism responsible for loss of interdigitated bone.

1. Introduction

Total knee replacement (TKR) is currently a very successful treatment option for most patients with knee arthritis. The major cause for revision surgery in cemented total knee arthroplasty is aseptic loosening of the tibial component. The mechanisms leading to this aseptic loosening are multi-factorial in nature and are not yet fully understood. Both biological and mechanical factors have been recognized to contribute toward peri-prosthetic osteolysis and eventual loosening and failure of TKRs (Gallo et al., 2013). Mechanical aspects such as early migration of tibial trays have previously been related to aseptic loosening (Pijls et al., 2012). Tibial component malalignment has also been shown to contribute toward revision rate due to increased wear (Srivastava et al., 2012). Patient factors such as activity levels and poor muscle condition can potentially lead to overloading of the knee joint.

In cemented knee arthroplasty, the purpose of bone cement is to provide an interlock between trabecular bone and cement, providing initial fixation of the implant to bone. An experimental study with cement-bone interface specimens from post-mortem tibial retrievals has however demonstrated a significant loss of trabecular bone at the bone-cement interface, with large gaps and increased interface micromotion. Considerable bone remodeling was also observed in the bone distal to the cement layer in the form of pedestal-shaped bony supports (Miller et al., 2014). A possible cause of loss of interdigitation is osteolysis induced by fluid flow and fluid pressure (Johansson et al., 2009; Fahlgren et al., 2010) at the tibial cement-bone interface (Mann and Miller, 2014). Micromotion between trabeculae and interdigitated bone cement could result in a fluid pumping mechanism leading to further degradation of bone. The large stiffness gradient across the implant-cement and cement-bone interfaces means that stress shielding of bone in cemented TKA will always occur, which in turn may lead to a reduction in trabecular bone density. The extent of stress shielding can possibly be mitigated by implant design and material optimizations

* Correspondence to: Orthopaedic Research Lab, Radboud university medical center, Huispost 547, PO Box 9101, 6500 HB Nijmegen, The Netherlands.
E-mail address: priyanka.srinivasan@radboudumc.nl (P. Srinivasan).

http://dx.doi.org/10.1016/j.jmbbm.2016.11.006
Received 23 June 2016; Received in revised form 12 October 2016; Accepted 1 November 2016
Available online 10 November 2016

and accurate cementation. To this end, it is necessary to understand how micromotion and strain are distributed in the interdigitated and peri-prosthetic bone. Using bone-cement interface specimens obtained from lab-prepared cemented tibial bones, finite element (FE) models were created to study variations in micromotion and bone strain. The pattern of strain shielding can be obtained by comparing post-operative bone strain with those in the pre-operative situation. Finite element modeling can be used to obtain the pre-operative strain distribution by removing the cement layer while keeping the loading condition the same. The purpose of this research is to investigate what changes occur at the cement-bone interface in terms of micromotion and strain due to cementation of the implant. The following research questions were therefore proposed: (1) How do micromotion and strain vary within the interdigitated trabeculae at the cement-bone interface post-operatively? (2) Is the interdigitated trabecular bone strain-shielded compared to the bone distal to the interface? (3) What is the extent of strain shielding at the cement-bone interface in the directly post-operative scenario compared to the (pre-operative) intact bone?

2. Materials and methods

The cement-bone interface specimens and resulting FE models used in this study have been described in a previous study (Srinivasan et al., 2016). The four FE models were validated based on experimental micromotion and strain measurements using Digital Image Correlation. In the section below, a brief description of the specimen creation and FE model generation is provided.

2.1. Specimen creation and FE model generation

Two fresh-frozen tibias obtained from the SUNY Anatomical Gift Program were prepared for cementation of tibial component as in TKR. Radiolucent surgical bone cement was vacuum mixed. After the cement reached a state of “does not stick to glove”, cement was applied to the proximal tibia and pressurized with a cement mixing spatula. Surgical bone cement (Radiolucent Simplex P, Stryker Orthopedics, Mawah, NJ) was vacuum mixed and applied to the proximal tibia once the cement had reached a state of *does not stick to glove*. Pressurization of cement into the trabecular bone was performed with a mixing spatula. Varying levels of cement interdigitation depth were obtained by applying twice as much cement to one half of the tibial plateau. The cemented tibias were sectioned into ~4×4×15 mm cement-bone interface specimens following a previously described method (Mann et al., 2008). From each donor, two specimens were chosen from tibial regions with different interdigitation depth (1.1–5.2 mm). These lab-prepared cement-bone specimens are representative of the immediate post-operative bone-cement interface.

Micro-CT scans of all specimens were made at 12 μm isotropic resolution (Scanco Inc. Media, PA, USA). The four cement-bone interface specimens were modelled using these micro-CT images. The images were segmented based on an image greyscale ranging from −1024 to −769 using Mimics 14.0 (Materialise, Leuven, Belgium). A threshold between −880 and −769 was applied for bone and between −1024 to −940 for cement. The segmentation mask of the cement layer was used to identify the interdigitated bone mask using the procedure described by Mann et al. (2012). Supporting bone was defined as bone distal to the cement layer (Fig. 1a) and was obtained by subtracting the interdigitated mask from the total bone mask. Segmentation masks of the cement, interdigitated bone and supporting bone were used to create corresponding surface and then 4-node tetrahedral solid meshes (3-matic 5.1 and Patran Mesher in Mentat 2012, MSC Software Corporation, Santa Ana, CA, USA). Due to the variation in cement interdigitation depth, the total number of elements ranged from 4 to 8 million with 1 to 2 million nodes. Specimen 1 had the least interdigitation depth and Specimen 4, the highest. The bone volume fraction (BV/TV) varied from 0.12 to 0.24 over the four specimens (Fig. 1a), which fall into the normal range for proximal tibial trabecular bone (Ding et al., 1999; Liu et al., 2008).

Linear elastic and isotropic material properties were assumed in the FE models. Young’s modulus for the cement and bone was set to 3 GPa (Lewis 1997) and 14 GPa, respectively. A Poisson’s ratio of 0.3 was applied for both materials. The cement-bone contact interface was modelled as unbonded (Waanders et al., 2010) and a double-sided segment-to-segment contact algorithm without friction was used (MSC Marc 2012). No influence of friction was seen in pilot studies.

The four (post-operative) models were loaded in compression at 1 MPa (which equated to 1 body weight) axially and constrained at both long ends, allowing only vertical movement (y-direction). Cement-trabecular micromotion was calculated using pairs of cement-bone contact nodes as described previously in the validation study. Each node pair was followed throughout the simulation, during which the total and incremental micromotion was calculated.

2.2. Pre-operative bone models

In order to obtain the change in strains once the implant has been cemented, it was needed to first recreate the pre-operative situation. This was done by cutting through the surface mesh of the cement (Rhinoceros 5.0) with a cutting plane; thereby effectively removing the cement layer. In each of the four models, the cut was performed such that just enough of the interdigitated cement geometry was preserved to form a pressure plate for the trabecular bone below (Fig. 1b). This ensured similar load distribution as in the post-operative situation. The surface mesh of the cement pressure plate was then converted to a solid tetrahedral mesh. The four new models - without interdigitated cement - represent the pre-operative situation. The same boundary conditions as in the post-operative models were applied to these models. The element sets and numbering for the bone was retained from the post-operative models so that change in strains could be obtained easily.

2.3. Definition ROI interdigitated bone

The main goal of this paper is to understand how micromotion and strain are distributed in the interdigitated bone post-surgery. To facilitate post-processing of relevant output variables, the elements and nodes of the interdigitated bone were divided into four regions of interest (ROI) having equal thickness (Fig. 2). The thickness of the regions between models was different due to the variation in depth of cement penetration. Regions were numbered 1–4, from most proximal to distal. Elemental strains and micromotion data were outputted using a subroutine. Median micromotion and strain were determined in each region and also as a function of interdigitation depth. Interdigitation depth is zero at the cement border and maximum at the deepest part within the cement mantle. The cement border is the distal border of the cement enclosing the interdigitated bone as shown in Fig. 2. Interdigitated bone strain (all four ROIs together) was also compared with supporting bone strain. The same ROIs were retained for the pre-operative models.

3. Results

3.1. Distribution of micromotion in interdigitated bone

Cement-trabecular micromotion was found to decrease from the distal to proximal interdigitated bone as shown in the FE contour plot for specimen 3 (Fig. 3). The contour plot shows the interdigitated bone without interdigitated cement layer for clarity. Maximum micromotion predicted by the four FE models was between 3 and 14 micrometers. Median micromotion in each region of interest as a function of the interdigitation depth showed that lower micromotion occurred deeper within the cement layer (Fig. 4). At the cement-bone contact interface

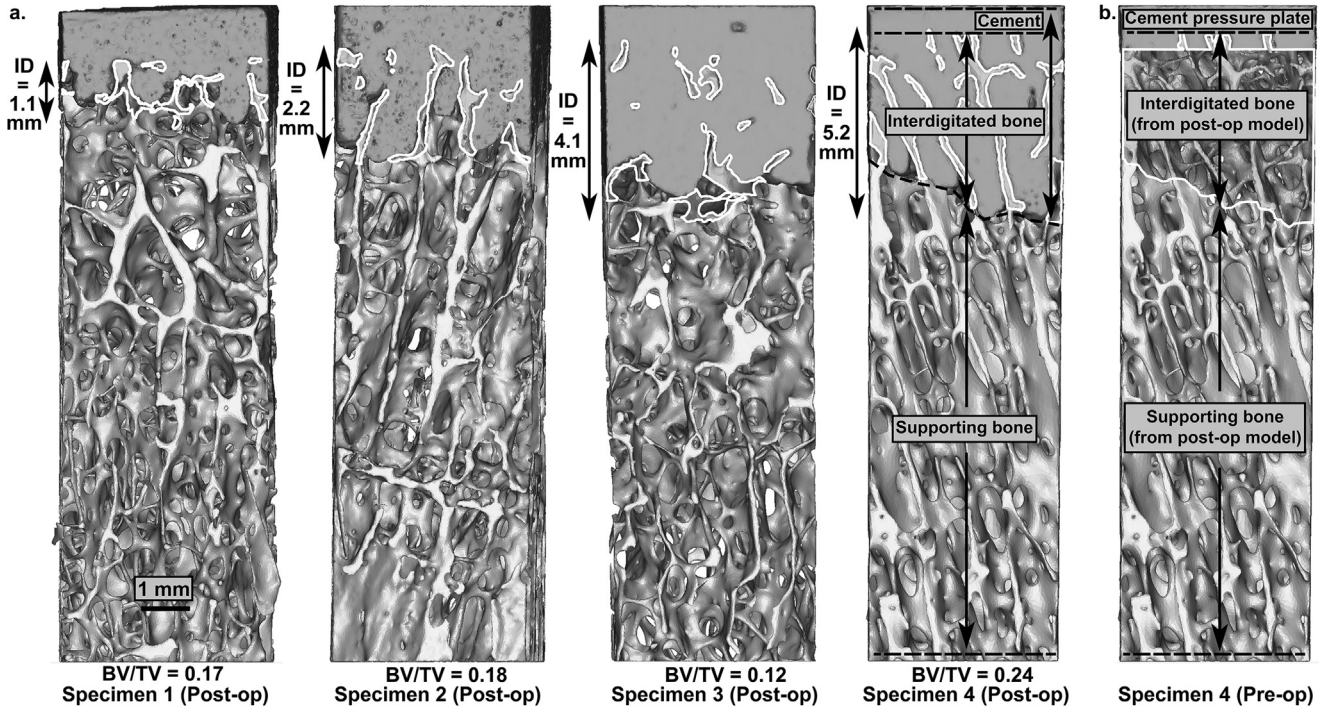

Fig. 1. Adapted from Srinivasan et al. (2016). FE models of the four specimens: (a) The four cement-bone interface FE models are representative of the immediately post-operative situation and have varying interdigitation depth (ID) and bone volume fraction (BV/TV). The white borders indicate the interdigitated bone. Element edges have not been shown for clarity. (b) The interdigitated cement mantle of model 4 has been removed to create the pre-operative situation. The same element sets for interdigitated bone and supporting bone were used in this pre-operative model.

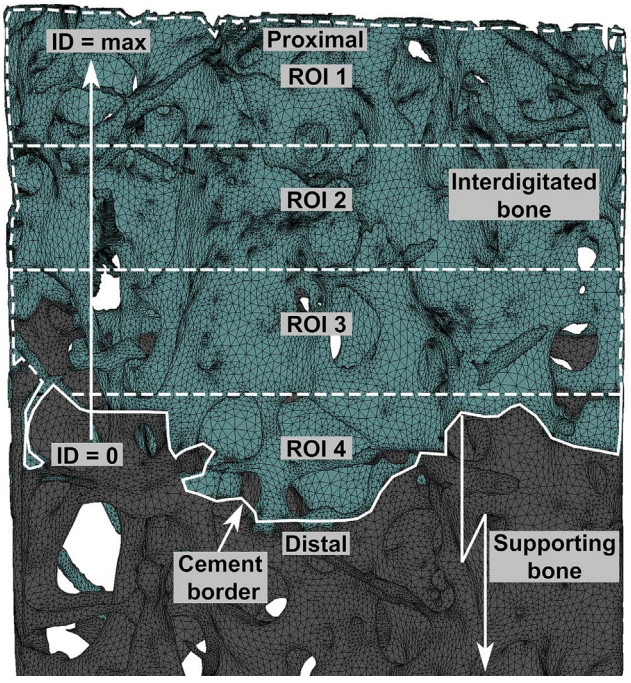

Fig. 2. Regions of interest within the FE models for micromotion and strain data: Interdigitated bone was further divided into four regions of interest (ROI) as shown here with specimen 3 as an example. The most proximal region was defined as having the maximum interdigitation depth (ID) and the most distal region, at the cement border (white solid line) has zero interdigitation depth. Supporting bone is all the bone distal to the cement border.

(interdigitation depth=0), a spread was seen in the micromotion. Interestingly, these differences coincided with the inter-specimen differences in BV/TV (i.e. specimens with a lower BV/TV displayed larger micromotion at the contact interface).

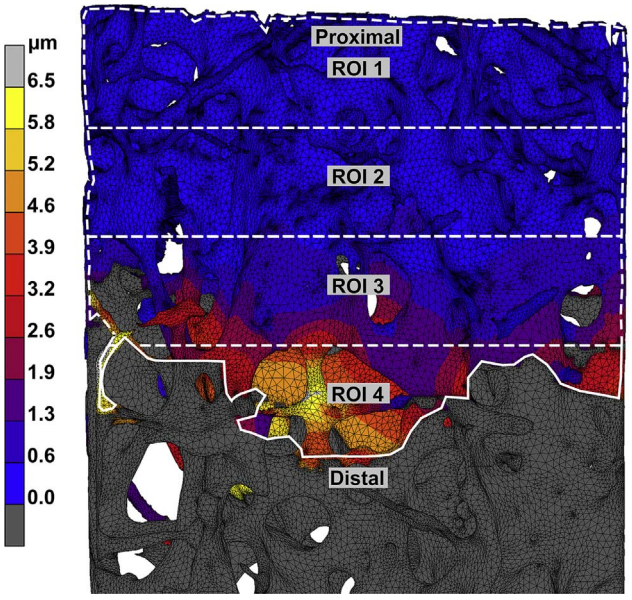

Fig. 3. Distribution of micromotion: micromotion contour plot of the interdigitated bone shows an increasing trend toward the cement border. The cement mantle is not shown for clarity. Micromotion values are in micrometers.

3.2. Distribution of strain in interdigitated trabecular bone

Interdigitated bone strain showed a similar decreasing trend from the most distal region through the most proximal region 4 for each specimen (Fig. 5). Interdigitated bone strain would be expected to be lower with increasing cement mantle thickness. Comparing the strain pattern of all four specimens, there was a general trend toward decreasing bone strain with increasing cement interdigitation depth. Specimen 3 is somewhat an exception to this trend, specifically in the more distal regions of interest.

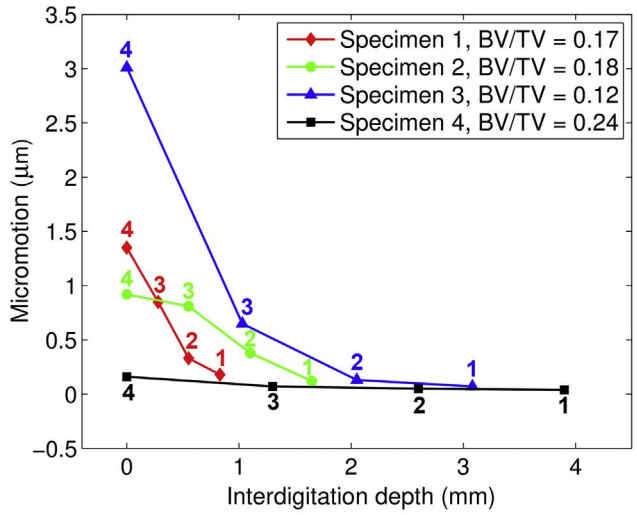

Fig. 4. Micromotion as a function of interdigitation depth: micromotion data obtained from the FE models are shown as median plots for the four regions of interest as a function of interdigitation depth. Marker numbers correspond to the defined regions of interest.

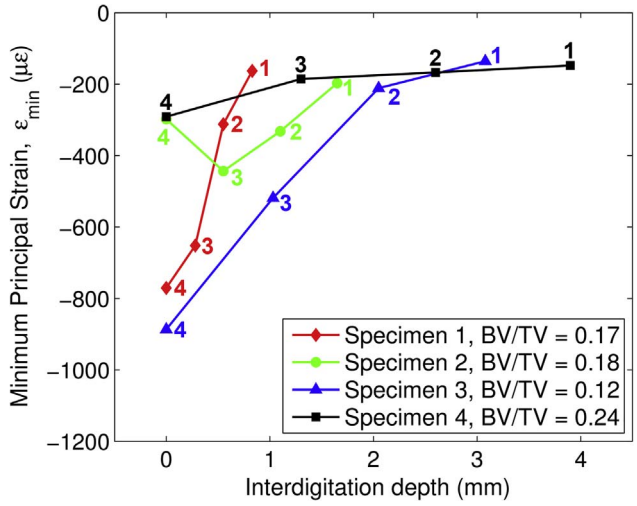

Fig. 5. Minimum principal strain as a function of interdigitation depth: median compressive strain showed a decreasing trend with increasing interdigitation depth when comparing the regions within each specimen. Marker numbers correspond to the defined regions of interest.

Median micromotion and strain values in each of the four interdigitated regions were tested using the Kruskal-Wallis test and were found to be significantly different from the other regions ($p < 0.01$). The same was true for all four specimens.

Again, when observing the strain at the contact interface only (interdigitation depth=0), strain tended to increase with decreasing BV/TV, indicating a possible effect of bone quality on bone load transfer in this region.

3.3. Interdigitated and supporting bone strain

Combining strain data for all regions of the interdigitated bone showed that the interdigitated bone was strain shielded compared to the supporting bone (Fig. 6a). The results are shown for one specimen; the same trend was observed for all specimens. Our results furthermore indicated that strain shielding increased with interdigitation depth, with a more evident difference in strain in regions 1, 2 and 3. The proximal part of the supporting bone (adjacent to region 4) was probably also strain shielded (Fig. 6b). Due to the morphology of the cement layer - and hence the resulting demarcation of interdigitated bone elements, there was some overlap between the proximal supporting bone and the distal interdigitated bone (see inlays Fig. 6b). Strain in the supporting bone alone was confirmed to have a strong correlation with bone volume fraction (r^2=0.87), as is to be expected.

3.4. Change in bone strain from pre-operative to post-operative

Fig. 7 shows the interdigitated bone strain for the pre-operative and post-operative situation. In general the difference in strain in the proximal regions was higher than in the more distal regions. Assuming that bone resorption was driven by strain shielding, this would indicate that maximum bone resorption occurs at region 1 and the least at region 4. Median percentage decrease in interdigitated bone strain in the cement-bone models was 59 %, 35 %, 61 % and 58 % respectively for the four specimens. As expected, there was very little change in supporting bone strain for all four specimens (< −3 % change in median value).

4. Discussion

This study investigated the distribution of cement-trabecular micromotion and trabecular bone strain in interdigitated trabeculae of lab-prepared cemented tibial tray specimens, with the aim to further elucidate the mechanism responsible for the bone resorption seen in post-mortem retrievals. Specimens having varying cement interdigitation depth and bone volume fraction were used to study the effect of specimen morphology on micromotion and strain.

Our results indicate that micromotion increased when progressing away from the implant, with the highest micromotion found at the cement border. This is in line with previous experimental findings with lab-prepared specimens (Miller et al., 2015), in which micromotion of similar magnitude were measured. The fact that the largest micromotion was found at the cement border would suggest that the majority of the bone resorption would occur in this region; however in post-mortem retrieved specimens this was shown not to be the case (Miller et al., 2015). In that particular study, analyses of tibial retrievals showed significant resorption in bone surrounded by cement, while at the cement border the bone remodeled to form pedestals to support the cement mantle. When a thicker cement mantle is present, the most proximal bone would get completely encapsulated in cement. It is possible that due to a lack of vascularity, the entrapped bone cannot be resorbed. This therefore indicates that fluid flow and high fluid pressure induced by cement-bone interface micromotion may not be the main cause for the bone resorption seen in the retrievals.

The strain analyses in the current simulations indicate that interdigitated bone at the tibial cement-bone interface is strain shielded. Similar to the micromotion, strain also showed an increasing trend when progressing away from the implant. Compared to the pre-operative situation (only bone models), the interdigitated bone in post-operative models displayed lower strains deeper in the cement, which indicates a potential for bone resorption in these regions (Fig. 7). Strain levels at the cement border differed to a lesser extent and may give an explanation for the pedestal support seen in post-mortem retrievals. These findings suggest strain adaptive remodeling may play an important role in the development of the cement-bone interface of cemented tibial trays. The results of this study are in agreement with the results presented by Zhang et al. (2016) where a micro-FE model of a bovine bone-cement interface specimen was used to determine the change in strain energy density as a result of using cemented fixation. They found that regions of interdigitated bone deeper within the cement mantle showed a greater potential for resorption. Reduction in strain energy density compared to the pre-operative state was above 95 % in the fully interdigitated regions of the interface. The partially interdigitated distal regions of the interface showed lower change in strain energy density. The results of this study confirm these findings

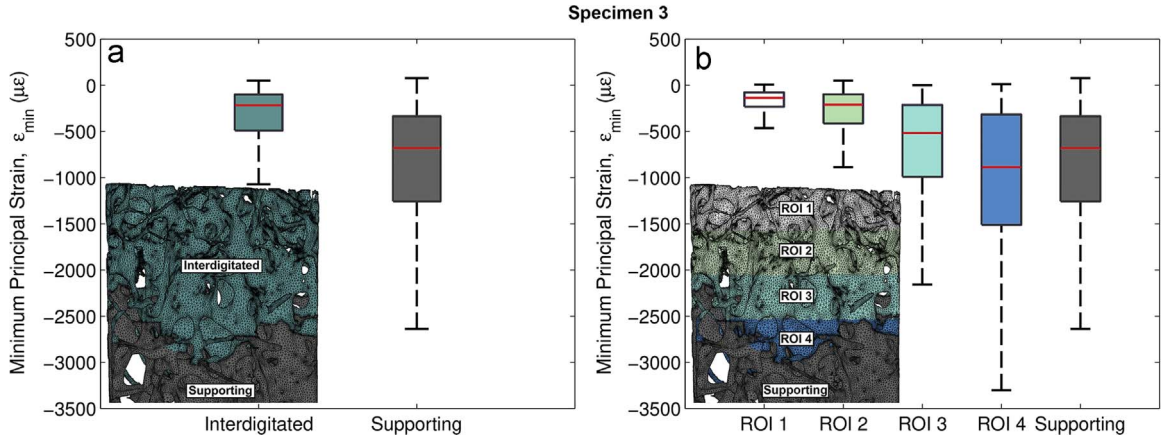

Fig. 6. Comparison of strains in interdigitated and supporting bone: (a) Compressive strains in the interdigitated bone were significantly lower than strains in the supporting bone. (b) Further comparison of the four regions of interest with the supporting bone shows the distribution of interdigitated bone strains compared to supporting bone strains.

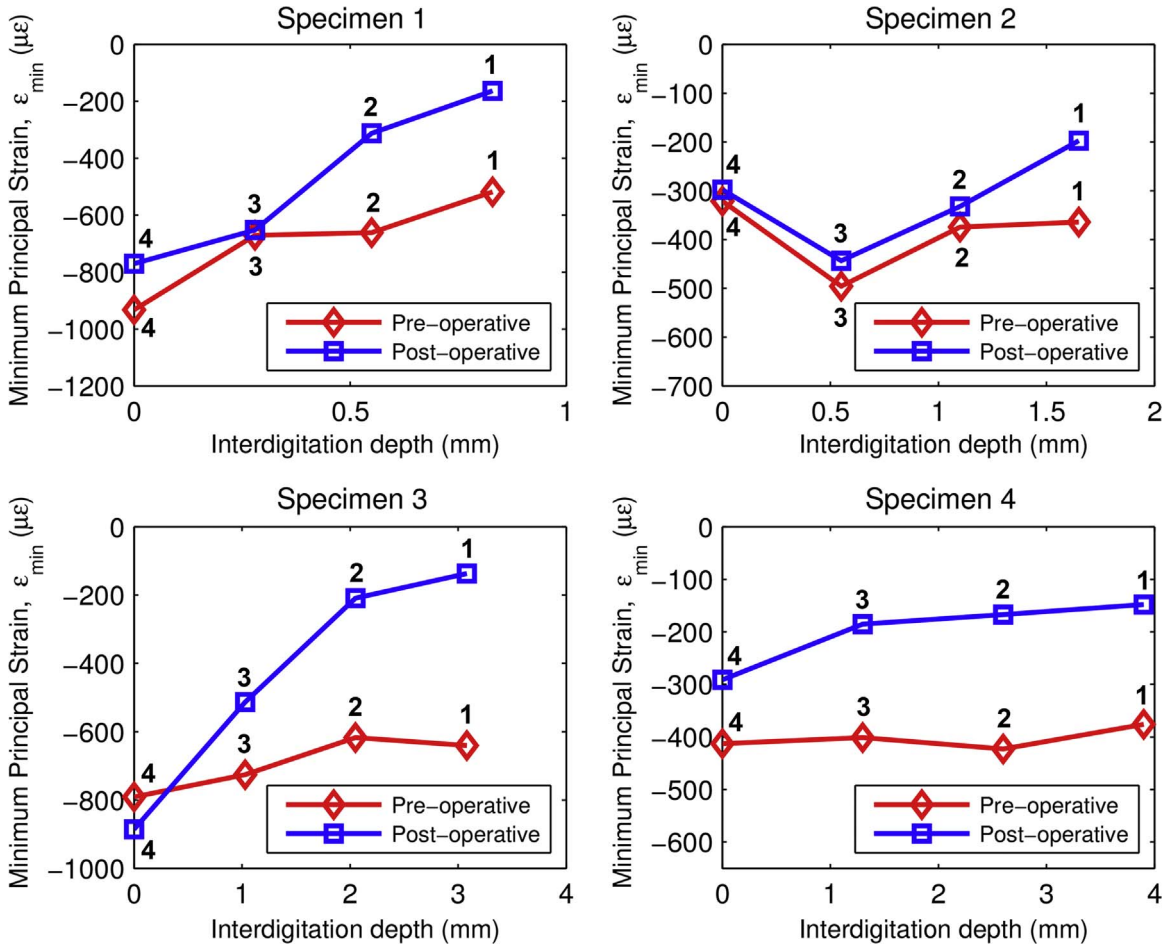

Fig. 7. Strain shielding of interdigitated bone: strain in the interdigitated bone before and after cementation show that bone is strain-shielded due to the presence of the cement layer. Marker numbers refer to the defined ROIs.

and further add to the current understanding of mechanical aspects of bone resorption and aseptic loosening by considering variations in specimen morphology.

Strains below the tibial tray have previously been measured in post-mortem retrieved tibias with cemented TKAs (Mann et al., 2014). Proximal (minimum principal) bone strains were higher than for the distal supporting bone in that study. The maximum regional bone strain measured on the outer cortical surface was 3000 με, which is similar to the maximum value (3300 με) predicted in ROI 4 of the interdigitated bone in Specimen 3 of this study (Fig. 6b). This value was higher than the maximum strain in the supporting bone (2600 με). This could indicate that some overloading of the bone may occur in the distal part of the interface in this specimen. As discussed by Mann et al. (2014), these strain values - when scaled up to the loads corresponding to normal walking, may exceed the yield strain for cortical and trabecular bone (7000 με).

Micromotion and strain would be expected to have some correlation with interdigitation depth. Results obtained in this study show, for all specimens, a decrease in micromotion and strain with increasing interdigitation depth (Figs. 4 and 5). Inter-specimen comparison of the

distal interface (ROI 4) revealed a large variation in micromotion and strain values. This variation cannot be fully explained as a dependence on interdigitation depth. However, there does appear to be a relationship between bone volume fraction and micromotion and strain values in ROI 4. The specimen with the largest bone volume fraction of 0.24 (specimen 4) had the lowest micromotion and strain; specimen 2 with the lowest bone volume fraction of 0.12 had the highest micromotion and strain in this region. Dependence of strain in the supporting bone on micro-structure (i.e. BV/TV) is to be expected, however, strain in the entire interdigitated bone – being strain shielded - would not be expected to demonstrate a clear dependence on bone volume fraction. The specific morphology of each specimen could also be a contributing factor to the relationship between BV/TV and distal interdigitated bone strain, but the demanding nature of cement-bone interface modelling limits the number of specimens that can be tested, validated and modeled. Specimen dimensions would also need to be larger to counter the effects of loss of continuity in the bone structure at the specimen edges. This would imply larger computational demands which are unfeasible at this time due to increasing contact area between bone and cement.

This study had a small number of specimens, each having varying morphological characteristics. The influence of any one characteristic on the interface properties therefore cannot be determined completely. Additional specimens analyzing the influence of variations in bone morphology, cement penetration depth and BV/TV would provide more information. However, simulations involving complex contact surfaces, as is the case here, are computationally quite demanding and time consuming. Patterns obtained for micromotion and strain were quite consistent and values were shown to increase when approaching the cement border. Moreover, the variations in micromotion and bone strain seen at the distal contact interface appeared to be related to the variation in bone morphology, stressing the importance of the use of actual cadaver tissue.

The tibial cement-bone interface undergoes mainly compressive forces, but depending on the implant type and specific location within the interface (e.g. around a keel), shear forces and/or a combination of shear and compression may be expected in the tibia. This study considered only compressive loads as this is the main load component. The specimens used here were previously tested experimentally in compression and comparison with other studies in compression was also made possible.

Our results indicate that strain adaptive remodeling is a plausible mechanism responsible for loss of interdigitated bone. In order to confirm these results, further studies will be focused on investigating post-mortem specimens which show varying levels of resorption.

5. Conclusions

Micromotion and strain patterns at the cement-bone interface were found to exhibit a reducing trend with increasing interdigitation depth. Interdigitated bone was demonstrated to be strain shielded in comparison with the underlying supporting bone using micro-FE models of interface specimens. The microstructure of proximal tibial trabecular bone in terms of bone volume fraction seemed to be related to the variation in micromotion and strain values at the distal interface. Strain shielding of interdigitated trabecular bone, in terms of reduction in compressive strain, was found to be between 35 % and 61 % for the four specimens used in this study. FE modelling is of particular use here as it offers the means to create models of the pre-operative scenario, which cannot be done experimentally using already cemented interface specimens.

Acknowledgements

Research reported in this publication was supported by the National Institute of Arthritis and Musculoskeletal and Skin Diseases of the National Institutes of Health, USA under Award Number AR42017. The content is solely the responsibility of the authors and does not necessarily represent the official views of the National Institutes of Health.

References

Ding, M., Odgaard, A., Hvid, I., 1999. Accuracy of cancellous bone volume fraction measured by micro-CT scanning. J. Biomech. 32 (3), 323–326.
Fahlgren, A., Bostrom, M.P.G., Yang, X., Johansson, L., Edlund, U., Agholme, F., Aspenberg, P., 2010. Fluid pressure and flow as a cause of bone resorption. Acta Orthop. 81 (4), 508–516.
Gallo, J., Goodman, S.B., Konttinen, Y.T., Wimmer, M.A., Holinka, M., 2013. Osteolysis around total knee arthroplasty: a review of pathogenetic mechanisms. Acta Biomater. 9 (9), 8046–8058.
Johansson, L., Edlund, U., Fahlgren, A., Aspenberg, P., 2009. Bone resorption induced by fluid flow. J. Biomech. Eng. 131 (9), 094505.
Liu, X.S., Sajda, P., Saha, P.K., Wehrli, F.W., Bevill, G., Keaveny, T.M., Guo, X.E., 2008. Complete volumetric decomposition of individual trabecular plates and rods and its morphological correlations with anisotropic elastic moduli in human trabecular bone. J. Bone Miner. Res. 23 (2), 223–235.
Mann, K.A., Miller, M.A., Cleary, R.J., Janssen, D., Verdonschot, N., 2008. Experimental micromechanics of the cement-bone interface. J. Orthop. Res. 26 (6), 872–879.
Mann, K.A., Miller, M.A., Pray, C.L., Verdonschot, N., Janssen, D., 2012. A new approach to quantify trabecular resorption adjacent to cemented knee arthroplasty. J. Biomech. 45 (4), 711–715.
Mann, K.A., Miller, M.A., Goodheart, J.R., Izant, T.H., Cleary, R.J., 2014. Peri-implant bone strains and micro-motion following in vivo service: a postmortem retrieval study of 22 tibial components from total knee replacements. J. Orthop. Res. 32 (3), 355–361.
Mann, K.A., Miller, M.A., 2014. Fluid-structure interactions in micro-interlocked regions of the cement-bone interface. Comput. Methods Biomech. Biomed. Eng. 17 (16), 1809–1820.
Miller, M.A., Goodheart, J.R., Izant, T.H., Rimnac, C.M., Cleary, R.J., Mann, K.A., 2014. Loss of cement-bone interlock in retrieved tibial components from total knee arthroplasties. Clin. Orthop. Relat. Res. 472 (1), 304–313.
Miller, M.A., Goodheart, J.R., Khechen, B., Janssen, D., Mann, K.A., 2015. Changes in microgaps, micromotion and trabecular strain from interlocked cement-trabecular bone interfaces in total knee replacements with in vivo service. J. Orthop. Res. 34 (6), 1019–1025.
Pijls, B.G., Valstar, E.R., Nouta, K.A., Plevier, J.W., Fiocco, M., Middeldorp, S., Nelissen, R.G., 2012. Early migration of tibial components is associated with late revision: a systematic review and meta-analysis of 21,000 knee arthroplasties. Acta Orthop. 83 (6), 614–624.
Srinivasan, P., Miller, M.A., Verdonschot, N., Mann, K.A., Janssen, D., 2016. Experimental and computational micromechanics at the tibial cement-trabeculae interface. J. Biomech. 49 (9), 1641–1648.
Srivastava, A., Lee, G.Y., Steklov, N., Colwell, C.W., Jr, Ezzet, K.A., D'Lima, D.D., 2012. Effect of tibial component varus on wear in total knee arthroplasty. Knee 19 (5), 560–563.
Waanders, D., Janssen, D., Verdonschot, N., Mann, K.A., 2010. The effect of cement creep and cement fatigue damage on the micromechanics of the cement-bone interface. J. Biomech. 43 (15), 3028–3034.
Zhang, Q.H., Cossey, A., Tong, J., 2016. Stress shielding in bone of a bone-cement interface. Med. Eng. Phys. 38 (4), 423–426.